



1 **Extending seasonal predictability of Yangtze River summer floods**

2 Shanshan Wang^{1,2}, and Xing Yuan¹

3 ¹Key Laboratory of Regional Climate-Environment for Temperate East Asia (RCE-TEA), Institute of
4 Atmospheric Physics, Chinese Academy of Sciences, Beijing, 100029, China

5 ²Key Laboratory of Arid Climatic Change and Reducing Disaster of Gansu Province, and Key Open
6 Laboratory of Arid Climate Change and Disaster Reduction of CMA, Institute of Arid Meteorology,
7 CMA, Lanzhou 730020, China

8 *Correspondence to:* Xing Yuan (yuanxing@tea.ac.cn)

9

10 **Abstract.** Extreme pluvial floods across China's Yangtze River basin in the summer of 2016 was
11 strongly connected with intense atmospheric moisture transport, and resulted in vast loss of properties
12 after a strong El Niño winter. Predicting such extreme floods in advance is essential for hazard
13 mitigation, but the flood forecast skill is relatively low due to the limited predictability of summer
14 precipitation. By using a “perfect model” assumption, here we show that atmospheric moisture flux has
15 a higher potential predictability than precipitation over the Yangtze River at seasonal time scales. The
16 predictability of precipitation and moisture are higher in post-El Niño summers than those in post-La
17 Niñas, especially for flooding events. As compared with extreme precipitation, the potential
18 detectability of extreme moisture increases by 20% in post-El Niño summers, which suggests that
19 atmospheric moisture could be crucial for early warning of Yangtze River summer floods.

20



21 1. Introduction

22 Located in eastern China with dense population and major agricultural and industrial productions, the
23 Yangtze River basin suffers from frequent flooding due to large interannual variability of the East Asian
24 summer monsoon. In June-July of 2016, extreme pluvial floods hit the middle and lower reaches of the
25 Yangtze River, caused severe inundations over many big cities, and resulted in direct economic loss of
26 70 billion RMB (about 10 billion U.S. dollars) (Yuan et al., 2018). Effective early warning of upcoming
27 extreme flood events is urgent to mitigate the potential damages, and strongly depends on accurate
28 precipitation forecasts not only at synoptic- but also subseasonal-to-seasonal scales (Yang et al., 2008;
29 Tian et al., 2017). However, predicting flood at seasonal time scales is still a grand challenge due to
30 limited forecast skill in precipitation at long leads (Alfieri et al., 2013; Yuan et al., 2015). This raises the
31 interests to explore other relevant variables that are more predictable than precipitation for flood early
32 warning.

33 Predictability is an inherent property of the climate system, and it represents the "ability to be predicted"
34 (Boer et al., 2013). As for a numerical prediction model, it is widely accepted that we cannot improve
35 the (precipitation) predictability without improving its dynamical framework, data assimilation and/or
36 physical parameterizations, etc (e.g., Barnston et al., 2012). However, most of the heavy precipitation
37 and flood events in many mid-latitude regions, especially in coastal areas, are strongly related to intense
38 horizontal atmospheric moisture transport (Ralph et al., 2006; Lavers et al., 2014). The atmospheric
39 moisture flux is supposed to be better predicted by large-scale climate models than precipitation that
40 might also be influenced by meso-scale convections (Lavers et al., 2014, 2016b). This provides a
41 potential to use atmospheric moisture flux to extend the predictability of floods. Recently, a series of



42 studies (Lavers et al., 2014, 2016a, 2016b) have assessed the varying predictability of precipitation and
43 moisture flux in winter, and shown that moisture flux yields a higher predictability than precipitation at
44 synoptic-scales (less than two weeks) across northwest Europe and western U.S. that are known as
45 affected by atmospheric rivers. At sub-seasonal to seasonal time scales, however, whether such
46 moisture and precipitation predictability relation also applies in China's monsoonal summer seasons
47 where convection is active, such as the Yangtze River summer flood, is still unclear.

48 The middle and lower reaches of the Yangtze region River basin in eastern China is one of the most
49 strongly El Niño-Southern Oscillation (ENSO)-affected regions in the world (e.g., Wang, 2000; Wu et
50 al., 2003; Ding and Chan, 2005). The persistent Sea Surface Temperature (SST) anomalies in the
51 equatorial Pacific can alter the tropical and subtropical circulation via local air-sea interaction and/or
52 teleconnections, and thus affect the East Asia summer climate significantly, including the summer
53 precipitation in Yangtze region. Such ENSO-related climate anomaly in Yangtze region is not
54 concurrent with the ENSO cycle, but at a season lag. A possible mechanism for this lag-impact of
55 ENSO on East Asia summer climate is the Indo-western Pacific ocean capacitor (IPOC), where the
56 North Indian Ocean warming after El Niño plays a crucial role (Xie et al., 2016). Therefore, the
57 precipitation predictability over the Yangtze River is closely associated with atmospheric and oceanic
58 conditions, which is similar to other regions (Gershunov, 1998; Kumar and Hoerling, 1998; Lavers et al.,
59 2016a). For instance, Kumar and Hoerling (1998) indicated that the North American climate is most
60 predictable during the late winter and early spring seasons of the warm ENSO events. Lavers et al
61 (2016a) showed that the moisture flux and extreme precipitation have different predictability during
62 different North Atlantic Oscillation (NAO) phases. In short, the weather or climate forecasts initialized



63 at different atmospheric/oceanic conditions can have varying levels of predictability, so understanding
64 how the Yangtze River rainfall predictability varies during different ENSO phases is also a concern.
65 In present study, we aim to address the above questions by evaluating the seasonal predictability of
66 precipitation and moisture flux for the middle and lower reaches of Yangtze River (110-123°E, 27-34°N)
67 based on multisource observational data, and ensemble hindcasts and real-time forecasts from a
68 dynamical seasonal forecast model Climate Forecast System version 2 (CFSv2; Saha et al., 2014) for
69 the period of 1982-2016.

70 2. Data and Method

71 2.1 Observation and reanalysis data

72 Monthly mean precipitation data at $1^\circ \times 1^\circ$ resolution over Yangtze River basin was obtained from
73 NOAA's precipitation reconstruction over land (PREC/L), which agrees well with gauge-based datasets
74 (Chen et al., 2002). Monthly mean atmospheric fields including geopotential height, u-wind, v-wind,
75 and specific humidity at different pressure levels were derived from the ERA-Interim reanalysis (Dee et
76 al., 2011). Herein, the mean June-July zonal and meridional atmospheric moisture fluxes between 300
77 and 1000 hPa were calculated separately, and their magnitudes were combined as the total moisture flux
78 (Lavers et al., 2016a).

79 NINO3.4 (5°S–5°N, 120°–170°W) SST anomaly based on ERSSTv4 monthly data (Huang et al., 2014)
80 during 1948–2016 was used to analyze the impact of ENSO on the seasonal predictability of rainfall
81 and moisture over the Yangtze River. An ENSO event was defined as the averaged NINO3.4 SST
82 anomaly during preceding December-January-February (DJF) exceeding its 0.5 standard deviation (σ).

83 2.2 CFSv2 seasonal hindcast and real-time forecast data



84 The ensemble hindcast and real-time forecast datasets including the monthly specific humidity and wind
85 field at different levels and monthly precipitation from Climate Forecast System version 2 (CFSv2)
86 (Saha et al., 2014), were used here to quantify the potential predictability. The predicted moisture flux
87 was calculated the same as the observation mentioned in Section 2.1. CFSv2 has 24 ensemble members
88 with different initial conditions (Yuan et al., 2011) and has been widely used for subseasonal to
89 seasonal forecasting (e.g., Kirtman et al., 2014; Yuan et al., 2015; Tian et al., 2017). All monthly
90 anomalies were calculated based on the climatology from entire hindcast period (1982-2010). The 0.5-
91 month lead forecast ensembles started from mid-May to early June (Saha et al., 2014), and predicted
92 through June-July. Similarly, the 1.5-month lead forecasts for the June-July started from the mid of
93 April, and so on.

94 **2.3 The potential predictability approach**

95 The potential predictability was quantified by using a “perfect model” assumption (Koster et al., 2000,
96 2004; Luo and Wood, 2006; Becker et al., 2013; Kumar et al., 2014; Lavers et al., 2016b). For the
97 predictions of June-July mean precipitation and moisture over each grid cell within Yangtze River basin
98 (110-123°E, 27-34°N) at a given lead time, ensemble member 1 was considered as observation and the
99 average of members 2–24 was taken as the prediction, which resulted in two time series with 35 years
100 of record (1982-2016). The skill of this forecast was then calculated by using the anomaly correlation

101 (AC; Becker et al., 2013) between these two time series, which is defined as $AC = \frac{\sum X'Y'}{[\sum (X')^2(Y')^2]^{1/2}}$, where

102 X' is the “observed” precipitation/moisture anomaly and Y' was the predicted counterparts. Here, the 95%
103 (90%) significant level is 0.33 (0.22) for AC according to a two-tailed Student’s t-test. Figure 1 gives an



104 example of the potential predictability calculation at a grid near Wuhan city, where the ensemble
105 member 1 was taken as the truth and the mean of the members 2-24 was the prediction. Result shows
106 that moisture has a higher predictability (AC) than precipitation at 0.5- and 1.5-month lead for member
107 1. This method was repeated 24 times, with each member being considered as the observation, so as to
108 obtain 24 AC values; the average of these 24 values was the final estimate of the potential predictability.
109 In addition to the calculation for individual grid cells, AC value was also calculated by using both
110 spatial and temporal samples for the Yangtze River basin with 72 CFSv2 grid cells. Here, an AC higher
111 than 0.05 would be considered as significant at 95% confidence level, both for ENSO events and the
112 entire period.

113 The rationale for this “perfect model” approach is that the statistical characteristics of the “observation”
114 (one of the ensemble members) and the prediction (ensemble mean of remaining members) are the same,
115 so the estimate of potential predictability is not affected by model biases (Kumar et al., 2014). Generally,
116 potential predictability is considered as the upper limit of forecasting skill, with an assumption that
117 internal physics or at least the statistical characteristics of observation and model prediction are
118 identical (Koster et al., 2004; Kumar et al., 2014).

119 In addition, the hit rate (HR) was also used to assess the seasonal predictability for extreme hydrologic
120 events (Ma et al., 2015), where the flooding condition was defined as the June-July mean precipitation
121 or moisture greater than 90th percentile of their climatology. Here, a forecast for flooding event can be
122 counted at a given grid or region when taking ensemble member 1 as observation and the average of
123 members 2–24 as the prediction: the HR was computed as $HR = \frac{a}{a+c}$, where a represents the number of
124 events that flooding is forecast and observed, b for flooding is forecast but not observed, and c for



125 observed flooding that is not forecast. Similar to the AC calculation, 24 HR values would be obtained
126 when each member was considered as the observation, and their average HR values was the final
127 potential predictability for extreme hydrologic events.

128 3. Results

129 3.1 Yangtze River 2016 pluvial flood and its associated atmospheric circulation

130 Figure 2a shows the spatial distribution of the 2016 June-July mean rainfall anomaly. Extreme pluvial
131 flooding hit the middle and lower reaches of Yangtze River, where the area averaged precipitation
132 increased by about 40% relatively to the climatology. In particular, continuous heavy rainfall
133 pummelled the Yangtze River basin, with rainfall anomalies locally exceeding 300mm within 10 days
134 (June 26-July 5; Yuan et al., 2018). Figure 2b shows that the June-July mean precipitation averaged
135 over the Yangtze River basin ranks only second to the 1954 flood during the period 1948-2016, and is
136 even heavier than the 1998 flood.

137 This Yangtze River extreme summer flood occurred in the context of the 2015/16 strong El Niño (Zhai
138 et al., 2016; Yuan et al., 2018). Generally, when the SST over the eastern tropical Pacific is warmer
139 than normal in the preceding winter, the Yangtze region would experience a wetter summer, or even a
140 flood hazard. For instance, the catastrophic flooding of the Yangtze River in the summer of 1998 was
141 strongly influenced by the 1997/98 extreme El Niño (e.g., Lau and Weng, 2001). From November 2015
142 to January 2016, the seasonal mean SST anomaly in the Niño 3.4 region (NOAA's Oceanic Niño Index)
143 peaked at 2.3 °C (L'Heureux et al., 2016), and returned to neutral condition until May 2016. With the
144 influence of the preceding El Niño signal, the western Pacific subtropical high (WPSH) was stronger
145 than climatology and located further west in the summer of 2016 through the Pacific-East Asian



146 teleconnection (e.g., Wang, 2000; Wu et al., 2003; Huang et al., 2007; Wang et al., 2014) and the Indo-
147 western Pacific Ocean capacitor (Xie et al., 2016), so a large amount of moisture was transported along
148 its western flank, from the Indian ocean, South China Sea and Pacific Ocean to the middle and lower
149 reaches of Yangtze River (Fig. 2c). As a result, there was a significantly anomalous moisture band in
150 the east-west direction characterized with the largest moisture transport amount in the middle and lower
151 reaches of Yangtze River, which was directly responsible for the 2016 summer flood (Fig. 2d).

152 **3.2 Seasonal predictability of precipitation and moisture flux**

153 Considering the association between intense moisture flux and heavy rainfall over the Yangtze River
154 basin, which is known within the canonical East Asian monsoon region (Ding and Chan, 2005), testing
155 whether atmospheric moisture is more predictable than precipitation at the seasonal time scale is helpful
156 for flood-control and disaster-relief. Figure 3 shows the predictions for June-July mean anomalies of
157 precipitation and corresponding moisture flux from the dynamical climate forecast model CFSv2 for the
158 2016 summer flood at the first three-month leads. As compared with the observed precipitation, CFSv2
159 successfully captured the rainfall surplus across the middle and lower reaches of the Yangtze River at
160 0.5-month lead (Fig. 3a), and predicted a visible moisture transport band along the middle and lower
161 reaches of the Yangtze River (Fig. 3b). The highest moisture anomaly occurred over the southern bank
162 of Yangtze River, which corresponded exactly to the location of heavy precipitation and flood. At 1.5-
163 month lead, CFSv2 still performed well for the anomalous moisture flux, but the predicted precipitation
164 anomaly was much weaker than that at the 0.5-month lead (Figs. 3c-3d). At the 2.5-month lead, the
165 prediction skill of precipitation significantly weakened with almost no anomaly (Fig. 3e), but the
166 predicted moisture could reproduce the anomaly to some extent (Fig. 3f).



167 In addition to the 2016 Yangtze flooding case, potential predictability for June-July precipitation and
168 moisture flux at different lead times during 1982-2016 is also investigated. Figures 4a-4f depict spatial
169 distribution of predictability for June-July mean precipitation and moisture flux at the 0.5-, 1.5- and 2.5-
170 month leads respectively, where moisture flux has higher predictability than precipitation. The highest
171 AC values for moisture flux occur over the south of the Yangtze River where frequently suffers from
172 extreme summer pluvial flooding. At the 0.5-month lead, the AC values for precipitation are lower than
173 0.3 over most areas (Fig. 4a), while they are higher than 0.3 and even close to 0.6 for moisture
174 predictability over the southern part of the Yangtze River basin (Fig. 4b). The AC value of precipitation
175 drops quickly over forecast leads, and more than half of the Yangtze region is less than 0.2 when
176 leading 1.5-month; but the moisture flux performs well with AC values higher than 0.3 and shows good
177 predictability in the southeast (Figs. 4c-4d). The moisture flux at the 2.5-month lead has higher AC
178 values even than precipitation at the 0.5-month lead (Fig. 4f). Meanwhile, it is evident that most areas of
179 the Yangtze River basin have significant predictability (at least at 90% confidence level) for the
180 moisture flux, but the predictability for precipitation is limited (Figs. 4a-4f).

181 Figure 4g indicates the corresponding spread for precipitation and moisture predictability throughout
182 the middle and lower reaches of Yangtze River region (110-123°E, 27-34°N). The median (mean) value
183 for precipitation is 0.25 (0.23) at the 0.5-month lead, but reaches 0.37 (0.35) for the moisture flux. At
184 the 2.5-month lead, the median (mean) value for moisture flux is 0.25 (0.24), which is much higher than
185 the value of 0.18 (0.16) for precipitation. The changes in potential predictability with different forecast
186 leads are also displayed in Figure 4h, based on both spatial and temporal samples for the Yangtze River
187 basin. It is evident that moisture flux has consistently higher predictability than precipitation out to 8.5-



188 month lead. Similar result is also found at the location (30°N, 114°E) near Wuhan city (Fig. 4i), one of
189 the big cities along the Yangtze River, which suffered widespread inundation in 2016.

190 **3.3 Varying predictability conditioned on different ENSO phases**

191 As mentioned above, the Yangtze region in eastern China is one of the most strongly ENSO-affected
192 regions in the world, and the precipitation variability in this region is generally influenced by the
193 anomalous ENSO forcing (e.g., Wang, 2000; Wu et al., 2003; Ding and Chan, 2005). To explore their
194 covariability, here we performed a maximum covariance analysis (MCA, Bretherton et al., 1992) for
195 preceding December-January-February mean SST (120E-80W, 10S-60N) and June-July mean
196 precipitation (100E-150E, 10N-55N) fields from 1948 to 2016. It is found that the second mode (MCA2)
197 explains 23% variance and its corresponding SST anomaly pattern is very similar to the traditional
198 ENSO-like pattern with a warm anomaly over equatorial eastern Pacific and a horse-shoes cold
199 anomalies over the western tropical and central Northern Pacific (Fig. 5a). Meanwhile, its temporal
200 evolution is strongly correlated with the NINO3.4 SST anomaly ($r = 0.92$, black line in Fig. 5c).
201 Correspondingly, the summer precipitation in Yangtze region is above normal significantly (Fig. 5b).
202 Therefore, the Yangtze region is prone to experience a rainy or flooding summer if the SST over the
203 eastern tropical Pacific is warmer than normal in the preceding winter based on the analysis during the
204 period 1948-2016, whether the predictability varies during different ENSO phases should be
205 investigated.

206 To explore the impacts of preceding El Niño signals on Yangtze precipitation and moisture
207 predictability, correlations and hit rates conditional on different ENSO phases at different leads are
208 shown in Figure 6. It is found that the seasonal predictability of Yangtze summer rainfall and moisture



209 flux is much higher following El Niño years than La Niñas (Fig. 6a). The contrast during different
210 ENSO phases is more obvious for extreme events, and potential detectability of extreme moisture
211 increases by 20% in post-El Niño summers as compared with potential detectability of extreme
212 precipitation (Fig. 6b). Figure 6 also shows that predictability is high conditional on El Niños even out
213 to 6.5-month lead, which is consistent with previous studies. For instance, Sooraj et al. (2012) have
214 mentioned that forecasting seasonal rainfall anomalies over central tropical Pacific islands from El Niño
215 winter into the following spring/summer is skillful by using CFS, and Ma et al. (2015) have
216 demonstrated high predictability for seasonal drought over ENSO-affected regimes in southern China.
217 The exception for 3.5-month lead forecast (started in March) where predictability conditioned on La
218 Niña is slightly higher than El Niño (Fig. 6a) is perhaps related to the ‘spring predictability barrier’, but
219 such chaos disappears for extreme events (Fig. 6b).

220 Furthermore, CFSv2 predictions of atmospheric circulations associated with 500 hPa geopotential
221 height and 850 hPa wind and moisture flux are also investigated during different ENSO phases. As
222 shown in Figure 6c, there is an anomalously high pressure center over western subtropical Pacific,
223 implying that the WPSH is enhanced in post-El Niño summers. Such circulation pattern brings the
224 moisture from southern oceans to Yangtze River basin, which corresponds well with extreme
225 hydrologic events. On the contrary, preceding La Niña winters are favorable to a low pressure anomaly
226 in next summer, accompanied with an abnormal cyclonic circulation, and thereby preventing the
227 moisture from moving northwards to the Yangtze region (Fig. 6d). The contrast is even obvious at 6.5-
228 month lead forecasts (Figs. 6e-6f). Such predicted circulation discrepancy in different initial ocean



229 conditions largely determines higher predictability for extreme hydrologic events over middle and lower
230 reaches of the Yangtze River basin in post-El Niño summers (Hu et al., 2014).

231 4. Summary and Discussion

232 Previous studies have revealed that moisture flux has higher predictability than precipitation in weather
233 forecasts over the northwestern Europe and the western U.S., which is affected by westerlies and
234 narrow bands of enhanced moisture transport known as atmospheric rivers (Lavers et al., 2014, 2016b).
235 However, whether the atmospheric moisture is more predictable at seasonal time scales during a
236 summer monsoon region is still unclear. Based on seasonal ensemble predictions from NCEP's
237 operational CFSv2 model during 1982-2016, our results show that moisture flux has higher seasonal
238 predictability than precipitation over China's Yangtze River basin in summer. Moreover, the potential
239 predictability may change under different climatic conditions. The predictability is much higher when
240 initialized in warm ENSO conditions not only for precipitation but also for moisture. More importantly,
241 the moisture shows higher detectability (hit rate) than precipitation for extreme pluvial flooding events
242 following El Niño winters. The results suggest that it may be possible to extend the predictability of
243 Yangtze River summer floods and to provide more reliable early warning by using atmospheric
244 moisture flux predictions. However, to which degree that moisture flux is connected with precipitation
245 and floods might be model dependent. It is necessary to explore their connections in a multi-model
246 framework (e.g., NMME; Kirtman et al., 2014; Shukla et al., 2016).

247 This study extends previous findings on the predictability of precipitation and moisture at synoptic
248 scales (Lavers et al., 2014) to seasonal time scales, and from atmospheric river-affected regions to the
249 East Asian summer monsoon region. Given that the transport of atmospheric moisture from oceanic



250 source regions is important for extreme rainfall in monsoon regions (Gimeno et al., 2012), moisture flux
251 might also be useful for long-range forecasting over other areas affected by the monsoon and low-level
252 jets. In fact, extreme precipitation and floods are found to be associated with large-scale moisture
253 transport over the North American monsoon (Schmitz and Mullen, 1996) and the South American
254 monsoon (Carvalho et al., 2010) regions.

255 The higher moisture predictability largely arises from more predictable large-scale circulation (Li et al.,
256 2016), which strongly determines the moisture transport. Although precipitation variability is affected
257 by both large-scale moisture transport and localized process and features, such as condensation nuclei in
258 the atmosphere and lifting movement, it is expected that moisture transport could still be used as a
259 crucial source of predictability for flooding over monsoonal regimes, especially at long leads where
260 meso-scale convection is still unpredictable at seasonal time scales.

261

262 **Acknowledgement.** This work was supported by National Natural Science Foundation of China
263 (91547103, 41605055), and the National Key R&D Program of China (2016YFA0600403). The authors
264 thank Dr. Arun Kumar for helpful discussions. The authors acknowledge NCEP/EMC and IRI
265 (<http://iridl.ldeo.columbia.edu/SOURCES/.NOAA/.NCEP/.EMC/.CFSv2/>) for making the CFSv2
266 hindcast and real-time forecast information available.

267



268 **References**

- 269 Alfieri, L., Burek, P., Dutra, E., Krzeminski, B., Muraro, D., Thielen, J., and Pappenberger, F.: G1FAS-
270 global ensemble streamflow forecasting and flood early warning, *Hydrol. Earth Syst. Sci.*, 17,
271 1161-1175, 2013.
- 272 Barnston, A. G., Tippett, M. K., L'Heureux, M. L., Li, S., and DeWitt, D. G.: Skill of real-time seasonal
273 ENSO model predictions during 2002–11: Is our capability increasing? *Bull. Amer. Meteor. Soc.*,
274 93, 631-651, doi:10.1175/BAMS-D-11-00111.1, 2012.
- 275 Becker, E. J., van den Dool, H. M., and Pena, M.: Short-term climate extremes: Prediction skill and
276 predictability, *J. Clim.*, 26, 512-531, 2013.
- 277 Boer, G. J., Kharin, V. V., and Merryfield, W. J.: Decadal predictability and forecast skill, *Clim. Dyn.*,
278 41, 1817-1833, doi:10.1007/s00382-013-1705-0, 2013.
- 279 Bretherton, C. S., Smith, C., Wallace, J. M.: An intercomparison of methods for finding coupled
280 patterns in climate data, *J. Clim.*, 5, 541-560, 1992. Carvalho, L. M. V., Silva, A. E., Jones, C.,
281 Liebmann, B., Silva Dias, P. L., and Rocha, H. R.: Moisture transport and intraseasonal variability
282 in the South America Monsoon system, *Clim. Dyn.*, 46, 1865-1880, 2010.
- 283 Chen, M., Xie, P., Janowiak, J. E., and Arkin, P. A.: Global Land Precipitation: A 50-yr Monthly
284 Analysis Based on Gauge Observations, *J. Hydrometeor.*, 3, 249-266, 2002.
- 285 Dee, D. P., Uppala, S. M., Simmons, A. J. et al.: The ERA-Interim reanalysis: Configuration and
286 performance of the data assimilation system, *Q. J. Roy. Meteor. Soc.*, 137(656), 553-597, 2011.
- 287 Ding, Y. H., and Chan, J. C. L.: The East Asian summer monsoon: An overview, *Meteor. Atmos. Phys.*,
288 89(1), 117-142, DOI: 10.1007/s00703-005-0125-z, 2005. Gershunov, A.: ENSO influence on



- 289 intraseasonal extreme rainfall and temperature frequencies in the contiguous United States:
290 Implications for long-range predictability, *J. Clim.*, 11(12), 3192-3203, 1998,
- 291 Gimeno, L., Stohl, A., Trigo, R. M., Dominguez, F., Yoshimura, K., Yu, L., Drumond, A., Durán-
292 Quesada, A. M., and Nieto, R.: Oceanic and terrestrial sources of continental precipitation, *Rev.*
293 *Geophys.*, 50, RG4003, doi:10.1029/2012RG000389, 2012.
- 294 Hu, Z-Z., Kumar, A., Huang, B., et al.: Prediction Skill of North Pacific Variability in NCEP Climate
295 Forecast System, *J. Clim.*, 27(11), 4263-4272, 2014.
- 296 Huang, B., Thorne, P., Smith, T., Liu, W., Lawrimore, J., Banzon, V., Zhang, H., Peterson, T., and
297 Menne, M.: Further Exploring and Quantifying Uncertainties for Extended Reconstructed Sea
298 Surface Temperature (ERSST) Version 4 (v4), *J. Clim.*, 29, 3119-3142, 2015.
- 299 Kirtman, B. P., et al.: The North American multimodel ensemble: phase-1 seasonal-to-interannual
300 prediction; phase-2 toward developing intraseasonal prediction, *Bull. Am. Meteorol. Soc.*, 95,
301 585-601, 2014.
- 302 Koster, R. D., Suarez, M. J., and Heiser, M.: Variance and predictability of precipitation at seasonal-to-
303 interannual timescales, *J. Hydrometeorol.*, 1, 26-46, 2000.
- 304 Koster, R. D., Suarez, M. J., Liu, P., Jambor, U., Berg, A., Kistler, M., Reichle, R., Rodell, M., and
305 Famiglietti, J.: Realistic initialization of land surface states: Impact on subseasonal forecast skill, *J.*
306 *Hydrometeorol.*, 5, 1049-1063, doi:10.1175/JHM-387.1, 2004.
- 307 Kumar, A., Hoerling, M. P.: Annual cycle of Pacific–North American seasonal predictability associated
308 with different phases of ENSO, *J. Clim.*, 11(12), 3295-3308, 1998.



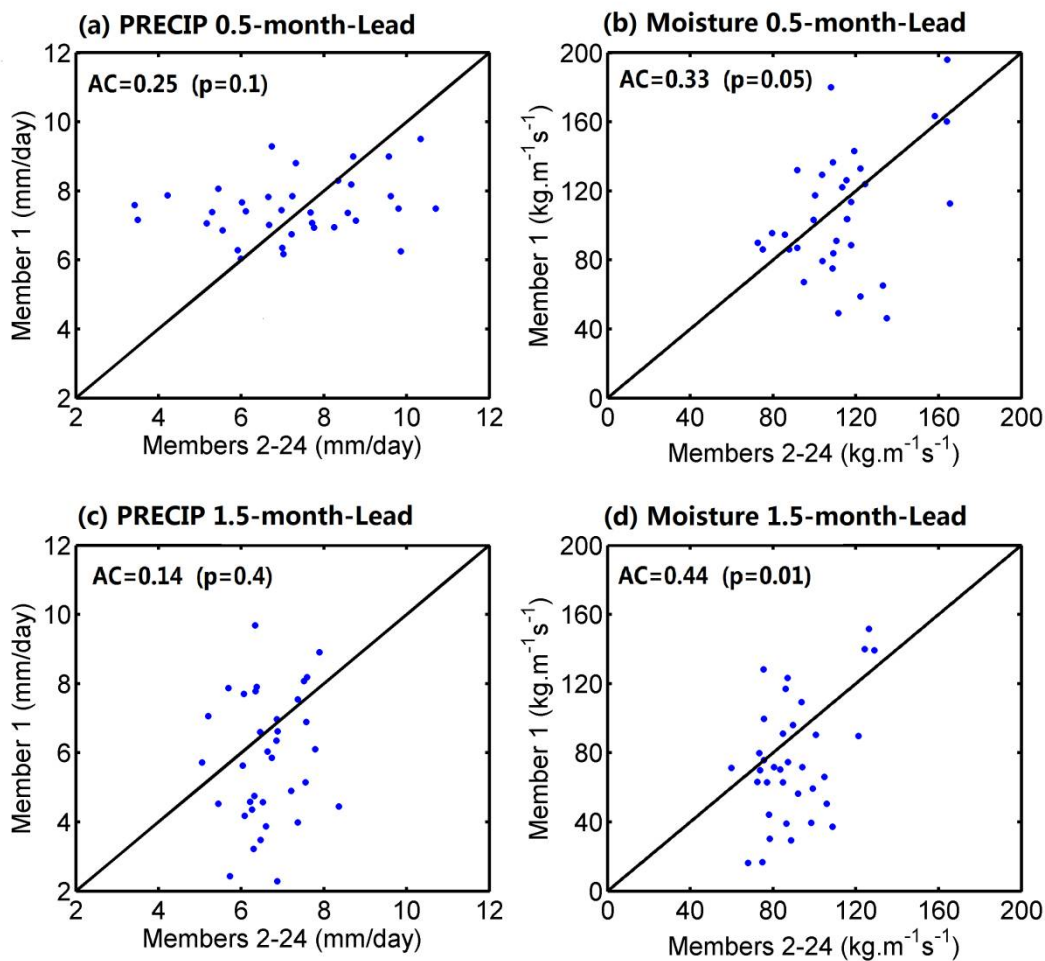
- 309 Kumar, A., Peng, P., and Chen, M.: Is there a relationship between potential and actual skill? Mon.
310 Weather Rev., 142, 2220-2227, 2014.
- 311 Lau, K. M., Weng, H.: Coherent modes of global SST and summer rainfall over China: An assessment
312 of the regional impacts of the 1997–98 El Nino, J. Clim., 14, 1294-1308, 2001.
- 313 Lavers, D. A., Pappenberger, F., and Zsoter, E.: Extending medium-range predictability of extreme
314 hydrological events in Europe, Nat. Commun., 5, 5382, 2014.
- 315 Lavers, D. A., Pappenberger, F., Richardson, D. S., and Zsoter, E.: ECMWF Extreme Forecast Index
316 for water vapor transport: A forecast tool for atmospheric rivers and extreme precipitation,
317 Geophys. Res. Lett., 43, 11852-11858, 2016a.
- 318 Lavers, D. A., Waliser, D. E., Ralph, F. M., and Dettinger, M. D.: Predictability of horizontal water
319 vapor transport relative to precipitation: Enhancing situational awareness for forecasting western
320 U.S. extreme precipitation and flooding, Geophys. Res. Lett., 43, doi:10.1002/2016GL067765,
321 2016b.
- 322 Li, C. F., Scaife, A., Lu, R. Y.: Skillful seasonal prediction of Yangtze river valley summer rainfall,
323 Environ. Res. Lett., 11(9), 094002, doi: 10.1088/1748-9326/11/9/094002, 2016.
- 324 Ma, F., Yuan, X., and Ye, A.: Seasonal drought predictability and forecast skill over China, J. Geophys.
325 Res. Atmos., 120, 8264-8275, doi: 10.1002/2015JD023185, 2015. L'Heureux, M. L., Takahashi,
326 K., Watkins, A. B., et al.: Observing and Predicting the 2015/16 El Niño, Bull. Amer. Meteor.
327 Soc., 98, 1363-1382, 2017.



- 328 Luo, L., and Wood, E. F.: Assessing the idealized predictability of precipitation and temperature in the
329 NCEP Climate Forecast System, *Geophys. Res. Lett.*, 33, L04708, doi:10.1029/2005GL025292,
330 2006.
- 331 Ralph, F. M., Neiman, P. J., Wick, G. A., et al.: Flooding on California's Russian River: Role of
332 atmospheric rivers, *Geophys. Res. Lett.*, 33, L13801, doi:10.1029/2006GL026689, 2006.
- 333 Saha, S., et al.: The NCEP climate forecast system version 2, *J. Clim.*, 27, 2185-2208, 2014.
- 334 Schmitz, J. T., and Mullen, S. L.: Water vapor transport associated with the summertime North
335 American Monsoon as depicted by ECMWF analyses, *J. Clim.*, 9, 1621-1634, doi:10.1175/1520-
336 0442(1996)009<1621:WVTAWT>2.0.CO;2, 1996.
- 337 Shukla, S., Roberts, J., Hoell, A., et al.: Assessing North American multimodel ensemble (NMME)
338 seasonal forecast skill to assist in the early warning of anomalous hydrometeorological events
339 over East Africa, *Clim. Dyn.*, 1-17, doi: 10.1007/s00382-016-3296-z, 2016.
- 340 Sooraj, K. P., Annamalai, H., Kumar, A., and Wang, H.: A Comprehensive Assessment of CFS
341 Seasonal Forecasts over the Tropics, *Wea. Forecasting*, 27, 3-27, [https://doi.org/10.1175/WAF-D-](https://doi.org/10.1175/WAF-D-11-00014.1)
342 11-00014.1, 2012.
- 343 Tian, D., Wood, E. F., and Yuan, X.: CFSv2-based sub-seasonal precipitation and temperature forecast
344 skill over the contiguous United States, *Hydrol. Earth Syst. Sci.*, 21, 1477-1490,
345 <https://doi.org/10.5194/hess-21-1477-2017>, 2017.
- 346 Wang, B., Wu, R., and Fu, X.: Pacific-East Asian teleconnection: How does ENSO affect the East
347 Asian climate? *J. Clim.*, 13, 1517-1536, 2000.

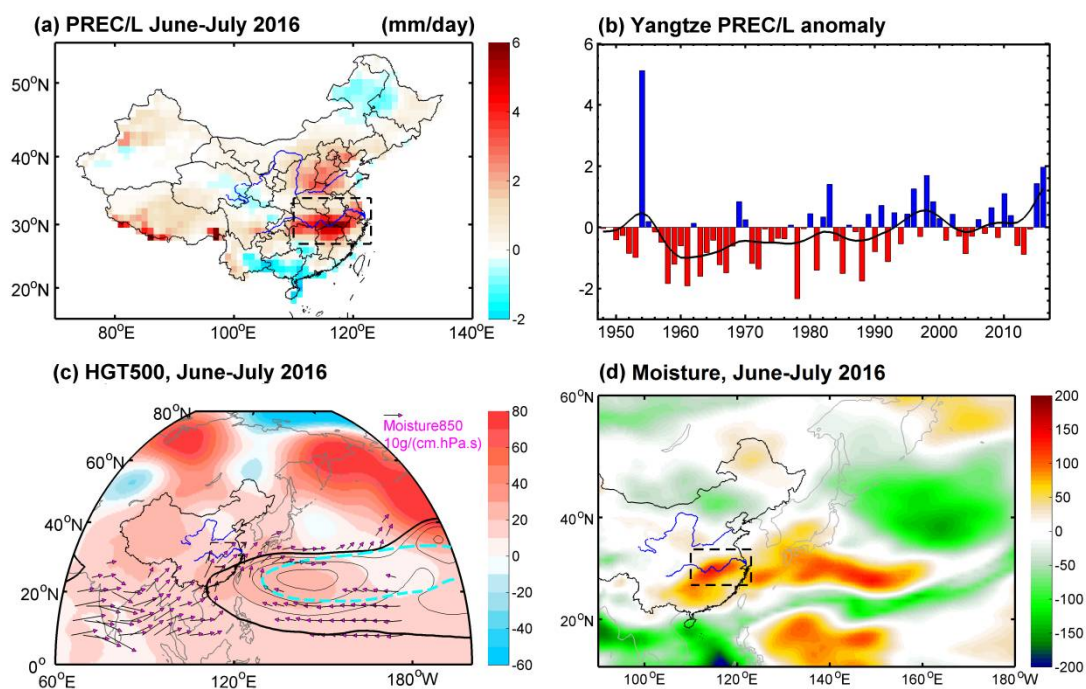


- 348 Wang, S., Huang, J., He, Y., Guan, Y. P.: Combined effects of the Pacific decadal oscillation and El
349 Nino-southern oscillation on global land dry–wet changes, *Sci. Rep.*, 4, 6651, 2014.
- 350 Wu, R., Hu, Z-Z., and Kirtman, B. P.: Evolution of ENSO-related rainfall anomalies in East Asia, *J.*
351 *Clim.*, 16, 3741-3757, 2003.
- 352 Xie, S-P., et al.: Indo-Western Pacific Ocean capacitor and coherent climate anomalies in post-ENSO
353 summer: A review, *Adv. Atmos. Sci.*, 33(4), 411-432, 2016.
- 354 Yang, S., Zhang, Z., Kousky, V. E., et al.: Simulations and seasonal prediction of the Asian summer
355 monsoon in the NCEP Climate Forecast System, *J. Clim.*, 21(15), 3755-3775, 2008.
- 356 Yuan, X., Wood, E. F., Luo, L., and Pan, M.: A first look at Climate Forecast System version 2 (CFSv2)
357 for hydrological seasonal prediction, *Geophys. Res. Lett.*, 38, L13402,
358 doi:10.1029/2011GL047792, 2011.
- 359 Yuan, X., Roundy, J. K., Wood, E. F., and Sheffield, J.: Seasonal forecasting of global hydrologic
360 extremes: system development and evaluation over GEWEX basins, *Bull. Am. Meteorol. Soc.*, 96,
361 1895-1912, 2015.
- 362 Yuan, X., Wang, S., and Hu, Z-Z.: Do climate change and El Niño increase likelihood of Yangtze River
363 extreme rainfall? *Bull. Am. Meteorol. Soc.*, 99, doi:10.1175/BAMS-D-17-0089.1, 2018.
- 364 Zhai, P., Yu, R., Guo, Y., et al.: The strong El Niño of 2015/16 and its dominant impacts on global and
365 China's climate, *J. Meteorol. Res.*, 30, 283-297, 2016.



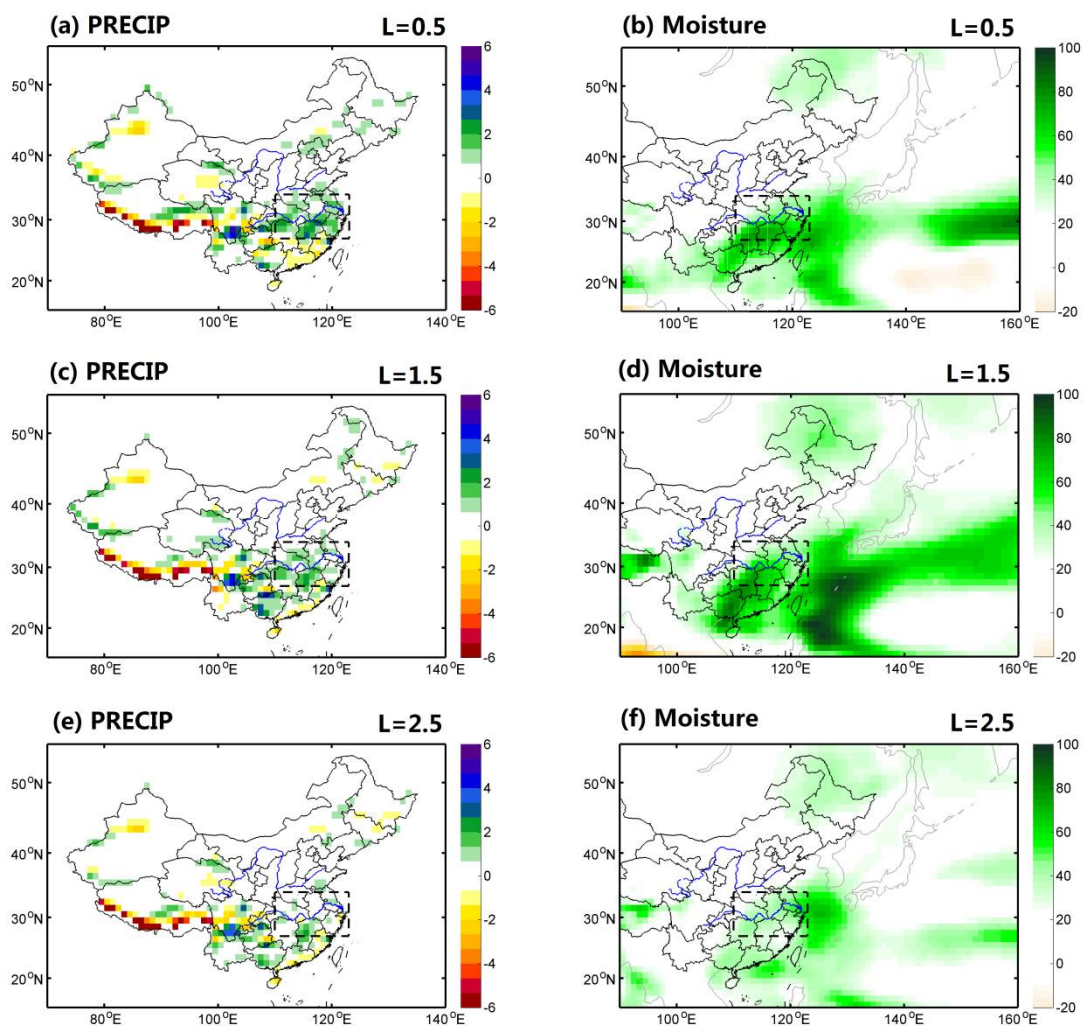
366

367 **Figure 1.** An example of the potential predictability calculation, where the ensemble member 1 is the
368 truth and the mean of the members 2-24 is the prediction. This is for 116°E and 28°N near to Wuhan
369 city at (a-b) the 0.5-month lead and (c-d) the 1.5-month lead.



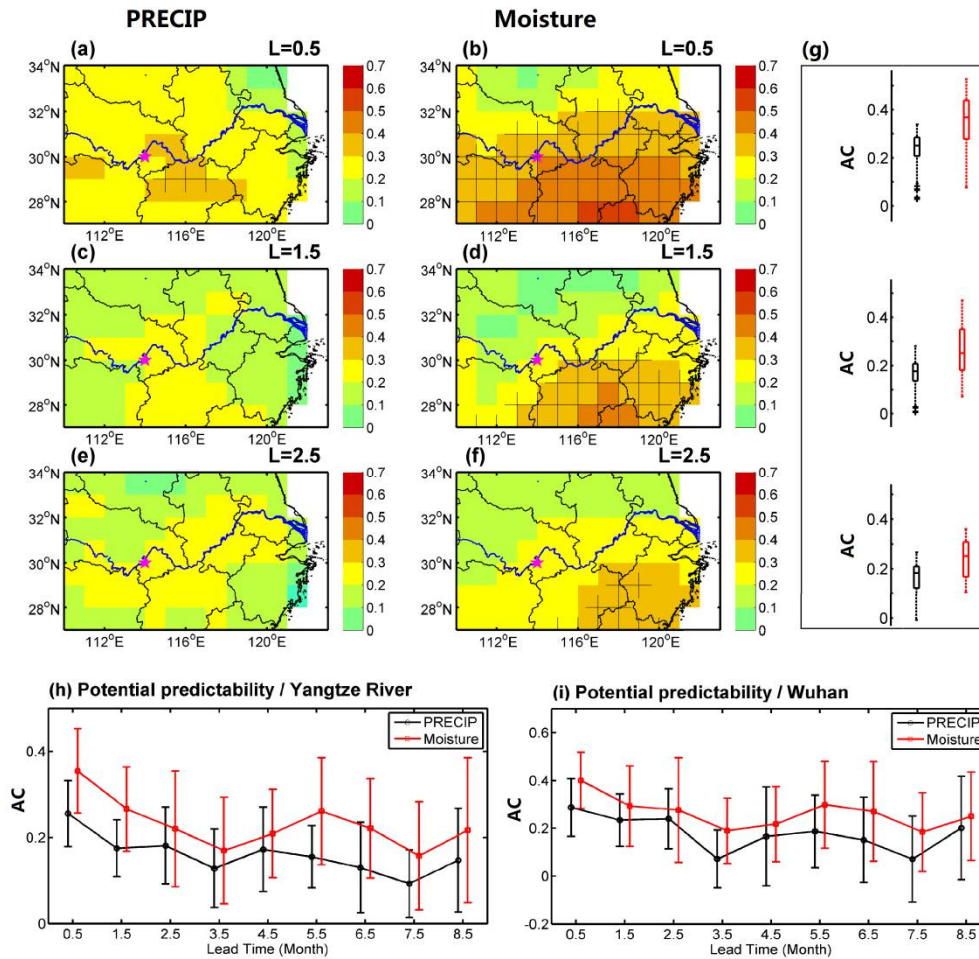
370

371 **Figure 2.** The 2016 extreme summer flood. (a) Mean precipitation anomaly (shading, mm/day) during
372 the June-July of 2016. (b) Time series of the June-July mean precipitation anomaly averaged over the
373 middle and lower reaches of Yangtze River basin (110-123°E, 27-34°N) in (a). (c) Anomaly of 500 hPa
374 geopotential height (shading, gpm) superimposed by absolute 850 hPa vapor transports (vectors,
375 g/cm·hPa·s). The thick contour lines are 5880 gpm, implying the location of the West Pacific
376 Subtropical High, where the black denotes the June-July 2016 and the cyan is the climatology during
377 1982-2010. (d) Anomaly of integrated horizontal moisture transport amount between 1000 to 300 hPa
378 layers (shading, Kg·m⁻¹s⁻¹).



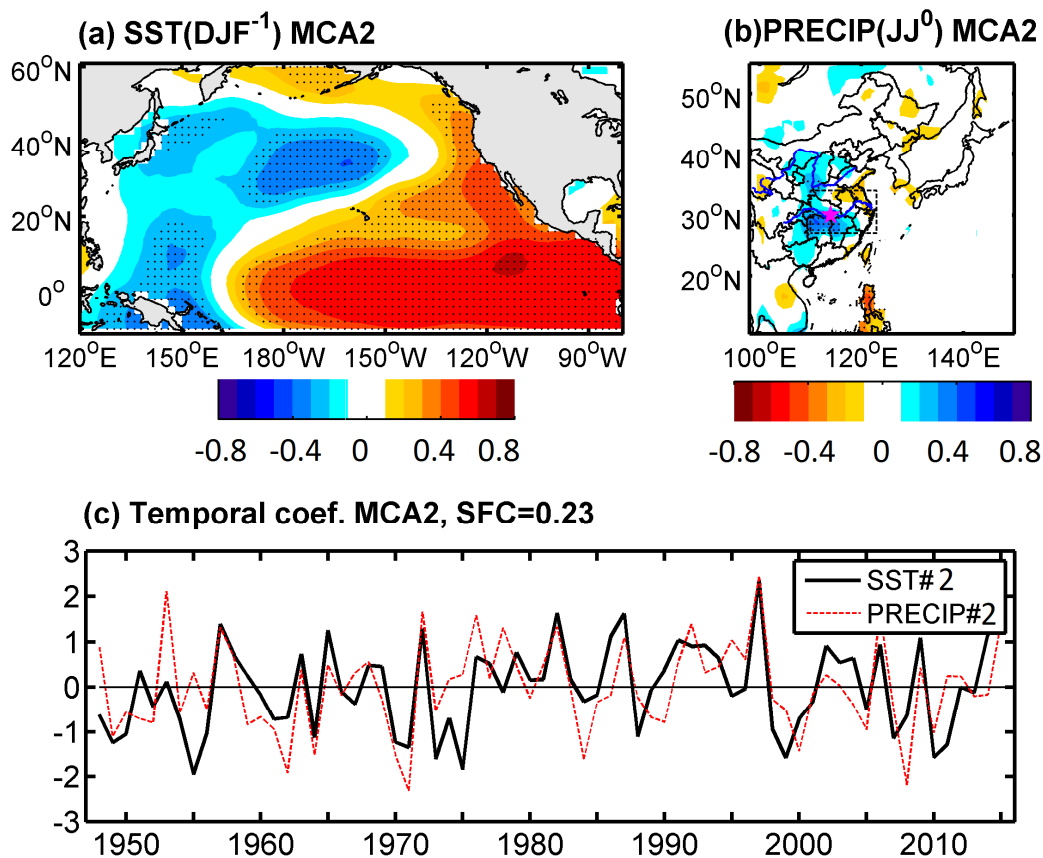
379

380 **Figure 3.** Spatial distributions of CFSv2 predicted anomalies of precipitation (shading, mm/day) and
381 atmospheric moisture flux (shading, $\text{Kg}\cdot\text{m}^{-1}\text{s}^{-1}$) in the June-July of 2016 at the 0.5-, 1.5- and 2.5-month
382 leads.



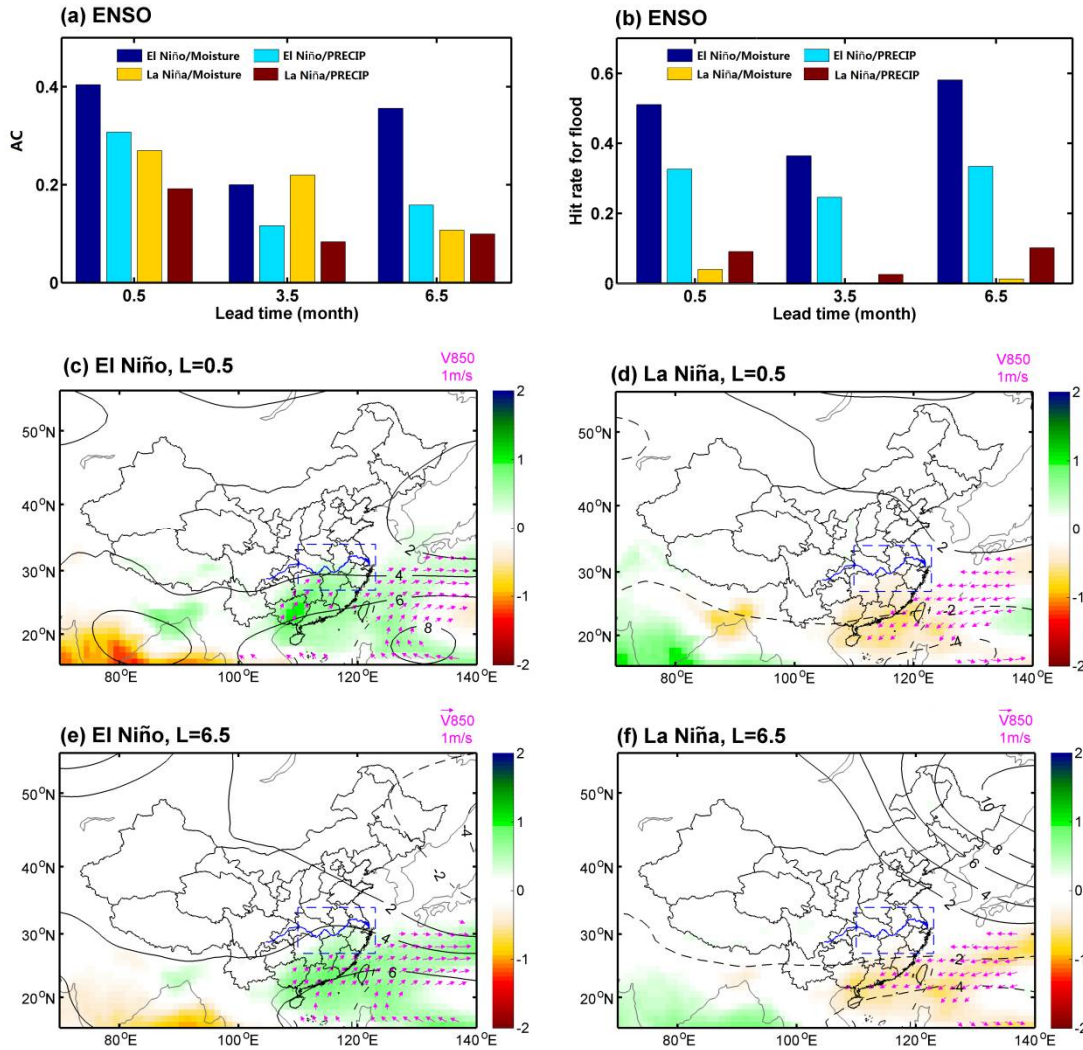
383

384 **Figure 4.** (a-f) Potential predictability (AC value, see Method) for June-July mean precipitation and
 385 atmospheric moisture flux at different lead times during 1982-2016 over the middle and lower reaches
 386 of Yangtze River for the 0.5-, 1.5- and 2.5-month leads; the stippling indicates a 95% confidence level
 387 according to a two-tailed Student's t-test. (g) Median, lower and upper quartiles, 1.5 times the
 388 interquartile ranges for AC values for precipitation (black) and moisture (red) throughout the study
 389 region (110-123°E, 27-34°N); outliers are displayed with + signs. (h-i) Potential predictability
 390 throughout study region and Wuhan city (pink pentagram in (a)) at different lead times; the error bars
 391 are standard deviations according to 24 members.



392

393 **Figure 5.** (a-b) Spatial and (c) temporal patterns of the second modes based on the maximum
394 covariance analysis (MCA) for SST in preceding winter (December-January-February) and
395 precipitation field in summer (June-July) for 1948-2016. Here the second MCA mode explains 23 % of
396 the variance, as indicated in the square fraction of covariance (SFC).



397

398 **Figure 6.** Potential predictability at different lead times in terms of (a) anomaly correlation (AC) for
 399 precipitation and moisture, and (b) hit rate (HR) for flood events (>90th percentiles) across the Yangtze
 400 River region conditioned on ENSO phases. (c-d) Composites of predicted anomalies of 500 hPa
 401 geopotential height (contour, gpm) superimposed by 850 hPa wind (vectors, m/s) and moisture flux
 402 (shading, $\text{g}/\text{cm}\cdot\text{hPa}\cdot\text{s}$) at the 0.5-month lead during different ENSO phases. (e-f) The same as (c-d), but
 403 for 6.5-month lead time.